Feature Comparisons Of 3-D Vector Fields Using Earth Mover's Distance

Rajesh Batra
Department of Aeronautics and Astronautics
Stanford University
Stanford, CA 94305

Lambertus Hesselink
Department of Electrical Engineering
Stanford University
Stanford, CA 94305-4035

1 Abstract

A method for comparing three-dimensional vector fields constructed from simple critical points is described. This method is a natural extension of the previous work [1] which defined a distance metric for comparing two-dimensional fields.

The extension to three-dimensions follows the path of our previous work, rethinking the representation of a critical point signature and the distance measure between the points. Since the method relies on topologically based information, problems such as grid matching and vector alignment which often complicate other comparison techniques are avoided. In addition, since only feature information is used to represent, and therefore stored for each field, a significant amount of compression occurs.

2 Introduction

Vector fields[1] are used to study phenomena in almost all areas of the physical sciences including such diverse subjects as climate modeling, dynamical systems, electromagnetism, and fluid mechanics. Hence, the analysis of vector fields has become a significant concern to the sciences, and a variety of techniques for visualizing and analyzing vector fields have been developed. However, an effective technique to quantitatively compare vector fields has not been developed. This paper addresses the issue.

A review of existing comparison techniques is first discussed. Even the most promising of these techniques lack the quantitative capabilities for automated comparisons. The properties of the two dimensional classification technique used in [1] are briefly discussed and are used to extend the classification to three-dimensional critical points. A complete categorization of 3-D simple critical points is presented and is used to redefine the EMD metric allowing for a quantitative comparison between 3-D flow fields. The paper concludes with an example demonstrating the effectiveness of

---

[1]The definition of vector fields is restricted to continuous fields or flows which are discussed in section 4.

the technique on a thermal convection model described by the Lorenz equations.

3 Existing Comparison Techniques

A variety of comparison techniques exist for vector fields. These techniques basically fall into three general categories: Image, data, and feature extraction based comparisons. In most of these cases, comparisons are made visually [2].

Image based comparisons work on the computer generated image. Often times, a numerical data set is converted into an image that simulates an experimental visualization technique (computational flow imaging). This may be easier than extracting a vector field from an image, such as Schlieren. However, visualizing a field in 3-D is quite difficult and often, these techniques are limited to two dimensions. In addition to side-by-side comparison of images, other techniques include image fusion, and Fourier analysis [3].

Data level comparison techniques operate directly on the raw data. An accurate comparison requires proper grid alignment which can involve problematic interpolation between two fields [4].

The last comparison category is the extraction of features. Typically features are problem specific; for example in fluid mechanics features include vortex cores and shock surfaces. Often there is a geometric representation of the feature and possibly a semantic representation of the system which can be compared using a pattern recognition technique [5]. This may lead to more robust comparisons.

Qualitative comparisons have been based on the concept of critical points in vector fields. Past study has focused on the geometric structure of vector fields [6] and last year a quantitative measure for two dimensional vector fields was introduced [1]. The work is extended by defining a quantitative measure of the similarities and differences of three-dimensional vector fields.

4 Description of Phase Portraits with 2-D α-β Parameters

Since the method reduces a 3-D flow pattern into 2-D components, the relevant 2-D categorization for this type of vector field is reviewed. A 2-D vector field that can be represented as a system of two simultaneous differential equations has the following form:

$$v_x = \frac{dx}{dt} = F(x, y) \tag{1}$$
$$v_y = \frac{dy}{dt} = G(x, y)$$

where F and G are continuous and have continuous partial derivatives in some region D. The solutions to this system forms a family of directed paths. Given some initial value to the system, a parametric representation expressed as $x = \phi(t)$, $y = \psi(t)$ can be deduced. The image formed is the phase portrait and is typically described by the number, type, and arrangement of critical points (or equilibrium points). These are points where $F(x, y) = 0$ and $G(x, y) = 0$. The nature of a critical point will not change under continuous (affine) transformation. Critical points are significant in that they are the only points in a vector field where tangent curves may cross each other. Therefore, critical points delineate the field into sectors of uniform flow.

A critical point is said to be isolated or simple if there is an open neighborhood around it that contains no other critical points. The behavior of the flow about a critical point can be analyzed by investigating the trajectories in the neighborhood of the critical point. If the distance is sufficiently small (say dx, dy), a first order approximation (Equation 2) of the field can be used.

$$v_x(dx, dy) \approx \frac{\partial v_x}{\partial x} dx + \frac{\partial v_x}{\partial y} dy \tag{2}$$
$$v_y(dx, dy) \approx \frac{\partial v_y}{\partial x} dx + \frac{\partial v_y}{\partial y} dy$$

Hence, the flow pattern is completely determined by the Jacobian, $J_{ij} = \frac{\partial v_i}{\partial v_j}$ ($i, j = 1, 2$) evaluated at the critical point. The various patterns formed in the phase-plane space can be seen by analyzing the eigenvalues of the Jacobian. The characteristic equation

$$\lambda^2 + P\lambda + Q = 0 \tag{3}$$

where $P = -trace(J)$ and $Q = det(J)$ is used to classify the various patterns using the well known $P - Q$ stability diagram [7]. However, advantageous properties arise by defining a new space (α', β') as explained in [1], where the eigenvalues map $\alpha = P$ and $\beta = sign(P^2 - 4Q)\sqrt{|P^2 - 4Q|}$
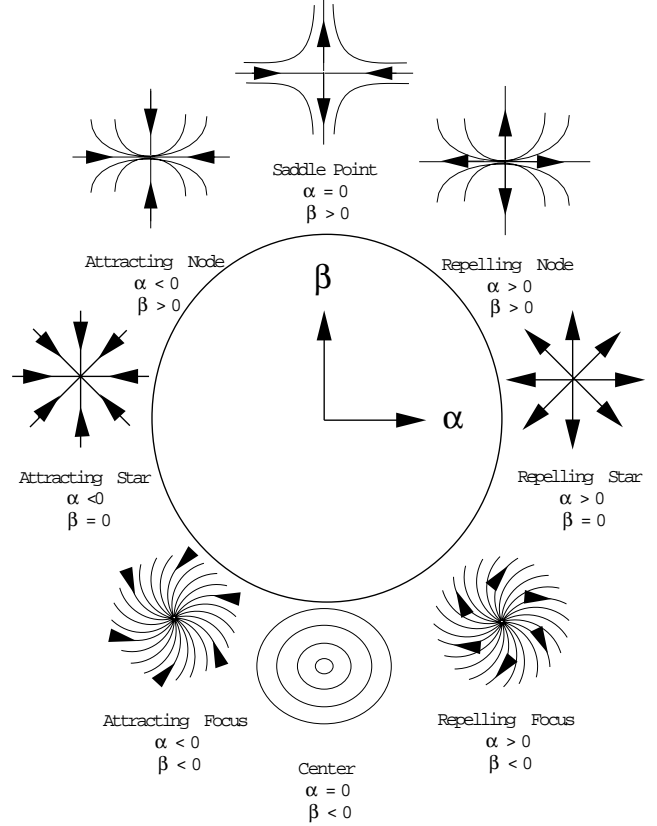
Figure 1: Basic patterns for simple critical points.

and are normalized as follows:

$$\alpha' = \frac{\alpha}{\sqrt{\alpha^2 + \beta^2}} \tag{4}$$
$$\beta' = \frac{\beta}{\sqrt{\alpha^2 + \beta^2}} \tag{5}$$

In this space, critical points obey all the the rules defined for a regular 2-D Euclidean space and the distance between any two critical points is a metric.

It is shown in [8] that the actual values of α and β do not determine the portrait of the critical point; only the ratio between them matters. Hence, this normalization maps all points onto a unit circle and thereby provides a means of relatively quantifying the difference between various points by just an angle. Also note that a uniform vector field with no critical points, $F(x, y) = c_1$, $G(x, y) = c_2$ has $\alpha = 0$ and $\beta = 0$ and maps to the origin of the unit circle. This is the reason why arc length is not used as a metric. For the remainder of the paper, α and β values will be assumed normalized. The patterns are sketched in Figure 1 and enumerated in Table 1 [2]. Notice a positive or negative real part

---

[2]The definition of saddle indicated in the table is more relaxed than spec-

α	β	Type	Constraint
> 0	$= 0$	Repelling Star	
> 0	> 0	Repelling Node	$|\beta| < |\alpha|$
—	> 0	Saddle	$|\beta| > |\alpha|$
< 0	> 0	Attracting Node	$|\beta| < |\alpha|$
< 0	$= 0$	Attracting Star	
< 0	< 0	Attracting Focus	
$= 0$	< 0	Center	
> 0	< 0	Repelling Focus	

Table 1: Classification of Critical Points via α-β values

(denoted by α) is indicative of repelling/attracting behavior. And if an eigenvalue has an imaginary part ($\beta < 0$), it indicates circulation about the point and the trajectories can be represented via logarithmic spirals, otherwise asymptotic behavior whose trajectories can be described via simple power laws is exhibited.

5 Classification of Three-Dimensional Vector Fields Using Phase Portraits

The formulation for a 3-D vector field is very similar to the 2-D analysis. For a three-dimensional vector field, the Jacobian is represented by a $3X3$ matrix, $J_{ij} = \frac{\partial v_i}{\partial v_j}$ ($i, j = 1, 2, 3$) The characteristic equation now becomes

$$\lambda^3 + P\lambda^2 + Q\lambda + R = 0 \qquad (6)$$

where $P = -trace(J)$, $Q = \frac{1}{2}(P^2 - trace(J^2))$, and $R = -det(J)$. Three distinct eigenvalues are possible, along with three eigenvectors. The flow field can be decomposed into fundamental solution trajectories along its eigenvector planes as demonstrated by Reyn [9] and Chong et al. [10]. All other solutions trajectories converge (or diverge) to these eigenvector planes. Therefore a critical point in 3-D can be defined by a set of three (α, β) values. Each (α, β) point corresponds to a solution trajectory formed in the respective eigenvector plane.

To simplify the classification of the various phase portraits about a three-dimensional critical point, the Jacobian is transformed into canonical form. This does not affect the eigenvalues since they are invariant to changes in scale, translation, and rotation. Philippou, and Strickland categorized the Jacobian into seven basic canonical forms [11] or classes. With each form, several phase-portraits are possible. In Tables 2 and 3, all possible cases are enumerated in a similar style as presented in reference [11] [3] along with the

ified in the figure.

[3]The class structure is slightly changed by placing the complex Jordan form last.
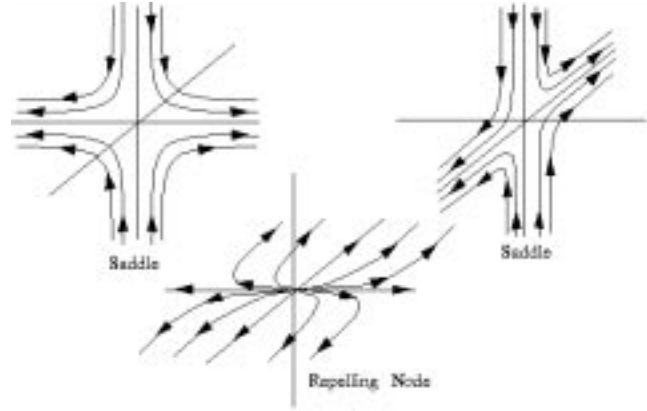
Figure 2: Decomposition of a class 1 critical point along eigenvector planes.

corresponding α, β sets. A brief discussion of the various classes is given below.

Class 1 $(\lambda_1, \lambda_2, \lambda_3)$: Class 1 is indicative of eigenvalues which are real and distinct. In this case, there exists three independent eigenvectors and therefore three independent eigenvector planes. For the case of a Hermitian matrix (and its subclass the real symmetric matrix), the eigenvectors are mutually orthogonal. If all of the eigenvalues are positive, repelling nodes form in all three planes. If the signs differ, a saddle occurs in two of the planes, and finally if all signs are negative attracting nodes occur. All other solution trajectories approach or diverge from the critical point as $t \to \infty$ and are not planar. In this case, there exists a full set of α, β values. A degenerate 2-D case is exhibited when one of the eigenvalues is zero. Only one plane will contain a simple solution trajectory, the other two planes will contain lines (since in 2-D every plane in the third dimension is identical). In this case, there exists only one distinctive α, β value. The remaining two are set to zero. In fact, all 2-D cases degenerate to $\{\{\alpha_1, \beta_1\}, \{0, 0\}, \{0, 0\}\}$ and the computed comparison values are identical to those in reference [1]. Figure 2 is an example of trajectories formed for a node/saddle/saddle combination.

Class 2 $(\lambda_1, \lambda_1, \lambda_2)$: This is a degenerate case where two eigenvalues are identical. The multiplicity is 2, however, 3 independent eigenvectors can still be found. One plane will contain a star pattern, the planes normal to this will contain solution trajectories (nodes or saddles) and will have identical α, β values. The 2-D case degenerates to the star pattern. The 1-D ($\lambda_1 = 0$) case is ignored.

Class 3 $(\lambda_1, \lambda_1, \lambda_2)$: In this case, only 2 independent eigenvectors and only two solution trajectories exist. In one plane, a log star [4] trajectory is observed and in the other plane

[4]A log star is also referred to as an improper node see [12]

a node or saddle. A log star in the α, β space is indistinguishable from a star pattern, i.e. $\alpha = \pm 1, \beta = 0$ since the star pattern is just a special case of the family of logarithmic stars formed.

Class 4 $(\lambda_1, \lambda_1, \lambda_1)$: Case 4 exhibits triple degeneracy with three independent eigenvectors. Any plane passing through the critical point will exhibit a star trajectory. The set of α, β values are identical.

Class 5 $(\lambda_1, \lambda_1, \lambda_1)$: Two linearly independent eigenvectors exist for this triple degeneracy case. Here there are only two independent planar trajectories. One trajectory is a log star located in the coordinate plane spanning the eigenvector (in x-y plane for the canonical form) and a star pattern in the other coordinate plane (x-z).

Class 6 $(\lambda_1, \lambda_1, \lambda_1)$: In this case, the multiplicity is three but only one independent eigenvector exists. Therefore, only one plane contains an attracting/repelling log star trajectory. Hence only one unique α, β value exists and this case conflicts with the 2-D case of class 2 and 3. Therefore, some false positives can be expected. Fortunately, class 1 is the most common occurrence [11], which this method classifies most uniquely.

Class 7 $(\alpha + \beta, \alpha - \beta, \lambda_3)$: Three eigenvalues are found, two of which must be complex conjugates of each other for the J matrix which contains no imaginary values. Only one plane will contain solution trajectories which are either a focus or a center. Hence, only one unique α, β pair value exists just as in the 2-D case. The real eigenvalue, λ_3, denotes a stretching or compressing phenomenon where trajectories either spiral away or towards the solution plane, and this will not be captured [13].

6 Feature Comparison via EMD

A flow field can now be described by a set of α, β values. To compare two flows, one approach is to find the closest match between the two sets of α, β values. The EMD algorithm provides this functionality. EMD is emphasized, since other techniques exist such as graph matching which takes into account connections between critical points. In the original description of EMD, terminology such as feature distribution, energy and work are used. The terminology is maintained for consistency and further information can be found in [14].

Earth Mover's Distance computes the minimal amount of work required to transform one distribution to another. In the case of vector fields, the distribution can be represented as the set of α, β values.

Definition 1 (Feature Distribution) *A feature distribution for a 3-D vector field is the set of sets of α and β values*

associated with the vector field's critical points:

$$\{\{(\alpha_1^{(1)}, \beta_1^{(1)}), (\alpha_2^{(1)}, \beta_2^{(1)}), (\alpha_3^{(1)}, \beta_3^{(1)})\},$$
$$\{(\alpha_1^{(2)}, \beta_1^{(2)}), (\alpha_2^{(2)}, \beta_2^{(2)}), (\alpha_3^{(2)}, \beta_3^{(2)})\},$$
$$\ldots, \{(\alpha_1^{(n)}, \beta_1^{(n)}), (\alpha_2^{(n)}, \beta_2^{(n)}), (\alpha_3^{(n)}, \beta_3^{(n)})\}\} \quad (7)$$

Definition 2 (Energy) *The energy for a vector field is:*

$$Energy = \sqrt{\sum_{j=1}^{n} \sum_{i=1}^{3} ((\alpha_i^{(j)})^2 + (\beta_i^{(j)})^2)},$$

where n is the total number of critical points in this field.

The energy is a quantity that characterizes the critical points of a vector field. It is different from physical energy. The concept "work" is used to measure the energy differences between two vector fields or the amount of energy used to transform one vector field into the other. For a 3-D vector field, work will be defined at two levels. At the higher level, the work required to convert one set of α, β values representing a critical point into another is needed. This is denoted as the Set Work. At the lower level, the work required to convert one α, β value in the set into another is needed. This will be defined as the Elemental Work. The Set Work is therefore the minimum amount of Elemental Work required to convert one set into another. Therefore, EMD can be used on the Set Work where the distance function is the Elemental Work.

Definition 3 (Set Work) *For two vector fields with feature distributions*

$$\{\{(\alpha_1^{(1)}, \beta_1^{(1)}), (\alpha_2^{(1)}, \beta_2^{(1)}), (\alpha_3^{(1)}, \beta_3^{(1)})\},$$
$$\{(\alpha_1^{(2)}, \beta_1^{(2)}), (\alpha_2^{(2)}, \beta_2^{(2)}), (\alpha_3^{(2)}, \beta_3^{(2)})\},$$
$$\ldots, \{(\alpha_1^{(n)}, \beta_1^{(n)}), (\alpha_2^{(n)}, \beta_2^{(n)}), (\alpha_3^{(n)}, \beta_3^{(n)})\}\}$$

and

$$\{\{(\hat{\alpha}_1^{(1)}, \hat{\beta}_1^{(1)}), (\hat{\alpha}_2^{(1)}, \hat{\beta}_2^{(1)}), (\hat{\alpha}_3^{(1)}, \hat{\beta}_3^{(1)})\},$$
$$\{(\hat{\alpha}_1^{(2)}, \hat{\beta}_1^{(2)}), (\hat{\alpha}_2^{(2)}, \hat{\beta}_2^{(2)}), (\hat{\alpha}_3^{(2)}, \hat{\beta}_3^{(2)})\},$$
$$\ldots, \{(\hat{\alpha}_1^{(n)}, \hat{\beta}_1^{(n)}), (\hat{\alpha}_2^{(n)}, \hat{\beta}_2^{(n)}), (\hat{\alpha}_3^{(n)}, \hat{\beta}_3^{(n)})\}\}$$

The amount of work necessary for transforming one vector field into the other is defined as:

$$Work_{set} = \sum_{i=1}^{n} EMD_e(\{(\alpha_1^{(i)}, \beta_1^{(i)})(\alpha_2^{(i)}, \beta_2^{(i)}), (\alpha_3^{(i)}, \beta_3^{(i)})\},$$
$$\{(\hat{\alpha}_1^{(i)}, \hat{\beta}_1^{(i)}), (\hat{\alpha}_2^{(i)}, \hat{\beta}_2^{(i)}), (\hat{\alpha}_3^{(i)}, \hat{\beta}_3^{(i)})\})$$
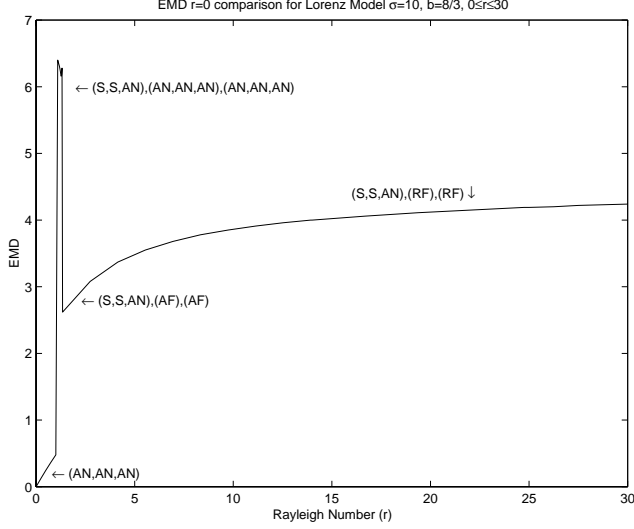
Figure 3: EMD capturing topological changes to Lorenz Model

where EMD_e is the Earth Mover's Distance whose distance function is the Elemental Work.

Definition 4 (Elemental Work) *For two vector fields with feature distributions*

$$\{(\alpha_1, \beta_1), (\alpha_2, \beta_2), \ldots, (\alpha_n, \beta_n)\}$$

and

$$\{(\alpha_1', \beta_1'), (\alpha_2', \beta_2'), \ldots, (\alpha_n', \beta_n')\}.$$

The amount of work necessary for transforming one vector field into the other is defined as: $Work_e = \sqrt{\sum_{i=1}^{n}((\alpha_i - \alpha_i')^2 + (\beta_i - \beta_i')^2)}$.

Notice that the definition for elemental work is identical to the work defined for a 2-D critical point defined in [1]. Since we decompose a 3-D critical point into a set of 2-D critical points, EMD at this lower level is the same as the 2-D case. To summarize, we can find the distance between two 3-D vector fields by extracting all 3-D critical points in the fields and representing them by a set of α, β values. Earth Mover's Distance is used to find the minimum energy between the critical points just as in the 2-D case. However, the distance metric is defined as the EMD over the *set* of α, β values whose distance metric is further defined as the elemental work. The elemental work is merely the Euclidean distance in α, β space and therefore is a metric. It can be shown that the Set Work is also a metric since EMD is a metric [14].

7 Example: Lorenz Model

One application for field comparisons is in the area of meteorology. Weather patterns can be searched for in a database to understand the development of a flow. E.N. Lorenz attempted to model thermally induced fluid convection in the atmosphere using the Navier-Stokes equations [15]. Using two-dimensional motion, fluid heated from below and cooled from above under the effects of gravity produce circulation or convection rolls. This phenomenon is summarized in Equation 8.

$$x' = \sigma(y - x) \tag{8}$$
$$y' = rx - y - xz$$
$$z' = -bz + xy$$

x(t) represents a measure of the fluid velocity (amplitude of the convection motion), and y(t), z(t) represent measures of the spatial temperature distribution. The equations are in non-dimensional form where σ is the Prandtl number (ratio of kinematic viscosity to thermal conductivity), b is a geometric factor and r is the Rayleigh number and is proportional to the temperature difference between the upper and lower regions of the system. These equations were one of the first to demonstrate chaotic behavior, and have resulted in over a hundred papers [16]. The resulting phase portrait of the system is in three-dimensions and is composed of simple critical points.

In the original study by Lorenz σ and b were fixed, and the Rayleigh number (i.e. the temperature difference between the plates) was varied. When r is below 1 only one critical point exists. As the temperature difference increases, three critical points form and eventually for large enough r the entire system becomes unstable. Using α, β space, the behavior of the system can clearly be seen and in fact the transformation from a stable system to an unstable system is continuous in this space.

Beginning with $r = 0$, Equation 8 has one critical point at the origin. As seen in Figure 4a, the critical point is type Class I whose phase portraits are three attracting (stable) nodes. As r is increased to 1, the angle measured from the positive α axis reduces and therefore the nodes become less stable as it nears the saddle point. The arrow in Figure 4a represents the critical point's progression with increasing r. At $r = 1$, the angle is 135° and a degenerate node forms (Figure 4b). Increasing r further, the origin's phase portrait becomes a set of two saddles, and an attracting node (Figure 4c). As r increases, the saddle points approach the repelling node.

In addition, for $r > 1$, two other critical points come into existence at $(\pm\sqrt{b(r-1)}, \pm\sqrt{b(r-1)}, r-1)$. For r near 1, another set of stable attracting nodes form (Figure 4d). However as r approaches 1.346, the angle increases

approaching an attracting star. Since the system is non-linear, the slightest perturbation causes the attracting star to become an attracting focus. Hence for $1.346 < r < 24.74$ (Figure 4e) an attracting focus forms. As r is increased to 24.76, the phase portrait changes gradually to a center. Hence, the observation of the unstable limit cycles forming around $r = 13.926$. Once r increases past 24.74, the angle increases to over 270° and a repelling focus comes into existence and the system is unstable.

The change with temperature can also be understood by observing how the phase portrait for a particular r compares with the remaining phase portraits. Figure 3 plots the EMD values required to change the critical points for $r = 0$ into other critical points at other r values. As can been seen, for $r < 1$, a gradual increase in EMD occurs as the attracting node at the origin becomes a saddle. As soon as $r > 1$, two new critical points form causing a large jump in EMD. The jump is drastic since six additional (2-D) critical points (attracting nodes) must form. Once $r > 1.346$, the phase portrait changes from three attracting nodes, to one attracting focus. Hence, less energy is required to create two additional focii than six critical points. From $r > 1.346$, the EMD value slowly increases as the system continuously moves further from a stable system to an unstable one. Not only is the attracting focii becoming a repelling focii, but the saddles at the origin are approaching degenerate repelling nodes (Figure 4c).

8 Conclusion and Future Work

We have extended the feature based comparison method to three-dimensional vector fields. We have shown that the extension can be straight-forward if we use the property that a 3-D critical point can be decomposed into a set of 2-D critical points with planar phase portraits. In addition, the redefined distance function for EMD remains a metric.

As with the 2-D case, connections between the critical points are not considered. Our experience has shown that for many cases this is sufficient, however, to reduce the number of false positives and to provide a better distance between two fields the connections should be taken into account. We are investigating this aspect along with generalizing this method to tensor fields.

This method has also demonstrated its usefulness in understanding complicated phenomenon such as the Lorenz model. The evolution of the thermal convection can be captured with EMD. Since the system is represented by quantities, fast searches can be easily constructed to locate particular patterns.

References

[1] Y. Lavin, R. Batra, and L. Hesselink, "Feature comparisons of vector fields using earth mover's distance," in *Proc. IEEE/ACM Visualization '98*, pp. 413–415, North Carolina, October 1998.

[2] F. H. Post and J. J. van Wijk, "Visual representations of vector fields: recent developments and research directions," in *Scientific Visualization* (L. Rosenblum, R. Earnshaw, and et al., eds.), pp. 181–195, Academic Press, Heidelberg, 1994.

[3] H.-G. Pagendarm and F. H. Post, "Comparative visualization-approaches and examples," in *Visualization in Scientific Computing* (M. Göbel, H. Müller, and B. Urban, eds.), pp. 95–108, Springer-Verlag, 1995.

[4] Q. Shen, A. Pang, and S. Uselton, "Data level comparison of wind tunnel and computational fluid dynamics data," in *Proc. IEEE Visualization '97*, pp. 67–74, CS Press, Los Alamitos, CA., 1997.

[5] L. Hesselink, "Digital image processing in flow visualization," *Annual Review of Fluid Mechanics*, vol. 20, pp. 421–485, 1988.

[6] J. Helman and L. Hesselink, "Representation and display of vector field topology in fluid flow data sets," *IEEE Computer*, vol. 22, pp. 27–36, Aug 1989. Also appears in *Visualization in Scientific Computing*, G. M. Nielson & B. Shriver, eds. Companion videotape available from IEEE Computer Society Press.

[7] A. Perry and B. Fairlie, "Critical points in flow patterns," *Advances in Geophysics B*, vol. 18, pp. 299–315, 1974.

[8] Y. Lavin, *Topology based visualization for vector and tensor fields*. PhD thesis, Stanford University, 1998.

[9] J. W. Reyn, "Classification and description of the singular points of a system of three linear differential equations," *Zeitschrift für angewandte Mathematik und Physik (ZAMP)*, vol. 15, pp. 540–557, July 1964.

[10] M. S. Chong, A. E. Perry, and B. J. Cantwell, "A general classification of three-dimensional flow fields," *Physics of Fluids A*, vol. 2, no. 5, pp. 765–777, 1990.

[11] P. A. Philippou and R. N. Strickland, "Vector field analysis and synthesis using three dimensional phase portraits," *Graphical Models and Image Processing*, vol. 59, pp. 446–462, November 1997.

[12] W. E. Boyce and R. C. DiPrima, *Elemetrary Differential Equations and Boundary Value Problems*. John Wiley & Sons, fourth ed., 1986.

[13] J. M. Chacín, B. J. Cantwell, and S. Kline, "Study of turbulent boundary layer structure using the invariants of the velocity gradient tensor," *Journal of Experimental Thermal and Fluid Science*, vol. 13, pp. 308–317, 1996.

[14] Y. Rubner and C. Tomasi, "The earth mover's distance as a metric for image retrieval," Tech. Rep. STAN-CS-TN-98-86, Department of Computer Science, Stanford University, September 1998.

[15] E. N. Lorenz, "Deterministic non-periodic flow," *J. Atmos. Sci.*, no. 20, pp. 130–141, 1963.

[16] C. Stoker, *The Lorenz Equations: Bifurcations, Chaos, and Strange Attractors*. Springer-Verlag, 1982.

Class	Canonical Form	Notes	Phase Portraits	$\|\alpha\|$	$\|\beta\|$
1	$\begin{bmatrix} \lambda_1 & 0 & 0 \\ 0 & \lambda_2 & 0 \\ 0 & 0 & \lambda_3 \end{bmatrix}$	Eigenvalues are real and distinct. Eigenvectors are linearly independent.	A-Node, A-Node, A-Node R-Node, R-Node, R-Node A-Node, Saddle, Saddle R-Node, Saddle, Saddle	$\alpha_1 = \frac{\lambda_1+\lambda_2}{\sqrt{2(\lambda_1^2+\lambda_2^2)}}$ $\alpha_2 = \frac{\lambda_1+\lambda_3}{\sqrt{2(\lambda_1^2+\lambda_3^2)}}$ $\alpha_3 = \frac{\lambda_2+\lambda_3}{\sqrt{2(\lambda_2^2+\lambda_3^2)}}$	$\beta_1 = \frac{\lambda_1-\lambda_2}{\sqrt{2(\lambda_1^2+\lambda_2^2)}}$ $\beta_2 = \frac{\lambda_1-\lambda_3}{\sqrt{2(\lambda_1^2+\lambda_3^2)}}$ $\beta_3 = \frac{\lambda_2-\lambda_3}{\sqrt{2(\lambda_2^2+\lambda_3^2)}}$
	$\begin{bmatrix} \lambda_1 & 0 & 0 \\ 0 & \lambda_2 & 0 \\ 0 & 0 & 0 \end{bmatrix}$	2-D case	A-Node R-Node Saddle	$\alpha_1 = \frac{\lambda_1+\lambda_2}{\sqrt{2(\lambda_1^2+\lambda_2^2)}}$ $\alpha_2 = 0$ $\alpha_3 = 0$	$\beta_1 = \frac{\lambda_1-\lambda_2}{\sqrt{2(\lambda_1^2+\lambda_2^2)}}$ $\beta_2 = 0$ $\beta_3 = 0$
2	$\begin{bmatrix} \lambda_1 & 0 & 0 \\ 0 & \lambda_1 & 0 \\ 0 & 0 & \lambda_2 \end{bmatrix}$	Eigenvectors are independent.	A-Star, A-Node, A-Node R-Star, R-Node, R-Node R-Star, Saddle, Saddle A-Star, Saddle, Saddle	$\alpha_1 = \pm 1$ $\alpha_2 = \frac{\lambda_1+\lambda_2}{\sqrt{2(\lambda_1^2+\lambda_2^2)}}$ $\alpha_3 = \frac{\lambda_1+\lambda_2}{\sqrt{2(\lambda_1^2+\lambda_2^2)}}$	$\beta_1 = 0$ $\beta_2 = \frac{\lambda_1-\lambda_2}{\sqrt{2(\lambda_1^2+\lambda_2^2)}}$ $\beta_3 = \frac{\lambda_1-\lambda_2}{\sqrt{2(\lambda_1^2+\lambda_2^2)}}$
	$\begin{bmatrix} \lambda_1 & 0 & 0 \\ 0 & \lambda_1 & 0 \\ 0 & 0 & 0 \end{bmatrix}$	2-D case	A-Star R-Star	$\alpha_1 = \pm 1$ $\alpha_2 = 0$ $\alpha_3 = 0$	$\beta_1 = 0$ $\beta_2 = 0$ $\beta_3 = 0$
	$\begin{bmatrix} 0 & 0 & 0 \\ 0 & 0 & 0 \\ 0 & 0 & \lambda_2 \end{bmatrix}$	1-D case	ignore	–	–
3	$\begin{bmatrix} \lambda_1 & 1 & 0 \\ 0 & \lambda_1 & 0 \\ 0 & 0 & \lambda_2 \end{bmatrix}$	Eigenvalues are real. 1 linearly dependent eigenvector.	A-Log Star, A-Node R-Log Star, R-Node R-Log Star, Saddle A-Log Star, Saddle	$\alpha_1 = \pm 1$ $\alpha_2 = 0$ $\alpha_3 = \frac{\lambda_1+\lambda_2}{\sqrt{2(\lambda_1^2+\lambda_2^2)}}$	$\beta_1 = 0$ $\beta_2 = 0$ $\beta_3 = \frac{\lambda_1-\lambda_2}{\sqrt{2(\lambda_1^2+\lambda_2^2)}}$
	$\begin{bmatrix} \lambda_1 & 1 & 0 \\ 0 & \lambda_1 & 0 \\ 0 & 0 & 0 \end{bmatrix}$	2-D case	A-Log Star R-Log Star	$\alpha_1 = \pm 1$ $\alpha_2 = 0$ $\alpha_3 = 0$	$\beta_1 = 0$ $\beta_2 = 0$ $\beta_3 = 0$
	$\begin{bmatrix} 0 & 1 & 0 \\ 0 & 0 & 0 \\ 0 & 0 & \lambda_2 \end{bmatrix}$	1-D case	ignore	–	–

Table 2: Phase Portraits for Classes 1,2,3. Legend: A- : Attracting R- : Repelling $\lambda_1 \neq \lambda_2 \neq \lambda_3 \neq 0$, $\lambda_1 > \lambda_2 > \lambda_3$

Class	Canonical Form	Notes	Phase Portraits	$\|\alpha\|$	$\|\beta\|$
4	$\begin{bmatrix} \lambda_1 & 0 & 0 \\ 0 & \lambda_1 & 0 \\ 0 & 0 & \lambda_1 \end{bmatrix}$	Eigenvalues are real. Eigenvectors are linearly independent.	A-Star, A-Star, A-Star R-Star R-Star, R-Star	$\alpha_1 = \pm 1$ $\alpha_2 = \pm 1$ $\alpha_3 = \pm 1$	$\beta_1 = 0$ $\beta_2 = 0$ $\beta_3 = 0$
5	$\begin{bmatrix} \lambda_1 & 1 & 0 \\ 0 & \lambda_1 & 0 \\ 0 & 0 & \lambda_1 \end{bmatrix}$	Eigenvalues are real. One linearly dependent eigenvector.	A-Log Star, A-Star R-Log Star, R-Star	$\alpha_1 = \pm 1$ $\alpha_2 = 0$ $\alpha_3 = \pm 1$	$\beta_1 = 0$ $\beta_2 = 0$ $\beta_3 = 0$
6	$\begin{bmatrix} \lambda_1 & 1 & 0 \\ 0 & \lambda_1 & 1 \\ 0 & 0 & \lambda_1 \end{bmatrix}$	Eigenvalues are real. Two linearly dependent eigenvectors.	A-Log Star R-Log Star	$\alpha_1 = \pm 1$ $\alpha_2 = 0$ $\alpha_3 = 0$	$\beta_1 = 0$ $\beta_2 = 0$ $\beta_3 = 0$
7	$\begin{bmatrix} \alpha & -\beta & 0 \\ \beta & \alpha & 0 \\ 0 & 0 & \lambda_3 \end{bmatrix}$	Two complex and one real eigenvalues.	A-Focus R-Focus Center	$\alpha_1 = \frac{\alpha}{\sqrt{\alpha^2+\beta^2}}$ $\alpha_2 = 0$ $\alpha_3 = 0$	$\beta_1 = \frac{\beta}{\sqrt{\alpha^2+\beta^2}}$ $\beta_2 = 0$ $\beta_3 = 0$

Table 3: Phase Portraits for Classes 4-7. Legend: A- : Attracting R- : Repelling $\lambda_1 \neq \lambda_2 \neq \lambda_3 \neq 0$, $\lambda_1 > \lambda_2 > \lambda_3$

Figure a: $0 \leq r < 1$

AN,AN,AN
$(x, y, z) = (0, 0, 0)$

Figure b: $r = 1$

DAN,DAN,AN
$(0, 0, 0)$

Figure c: $r > 1$

S,S,AN
$(0, 0, 0)$

Figure d: $1 < r < 1.346$

AN,AN,AN
$(\pm\sqrt{b(r-1)}, \pm\sqrt{b(r-1)}, r-1)$

Figure e: $1.346 < r < 24.74$

AF
$(\pm\sqrt{b(r-1)}, \pm\sqrt{b(r-1)}, r-1)$

Figure f: $r > 24.74$

RF
$(\pm\sqrt{b(r-1)}, \pm\sqrt{b(r-1)}, r-1)$
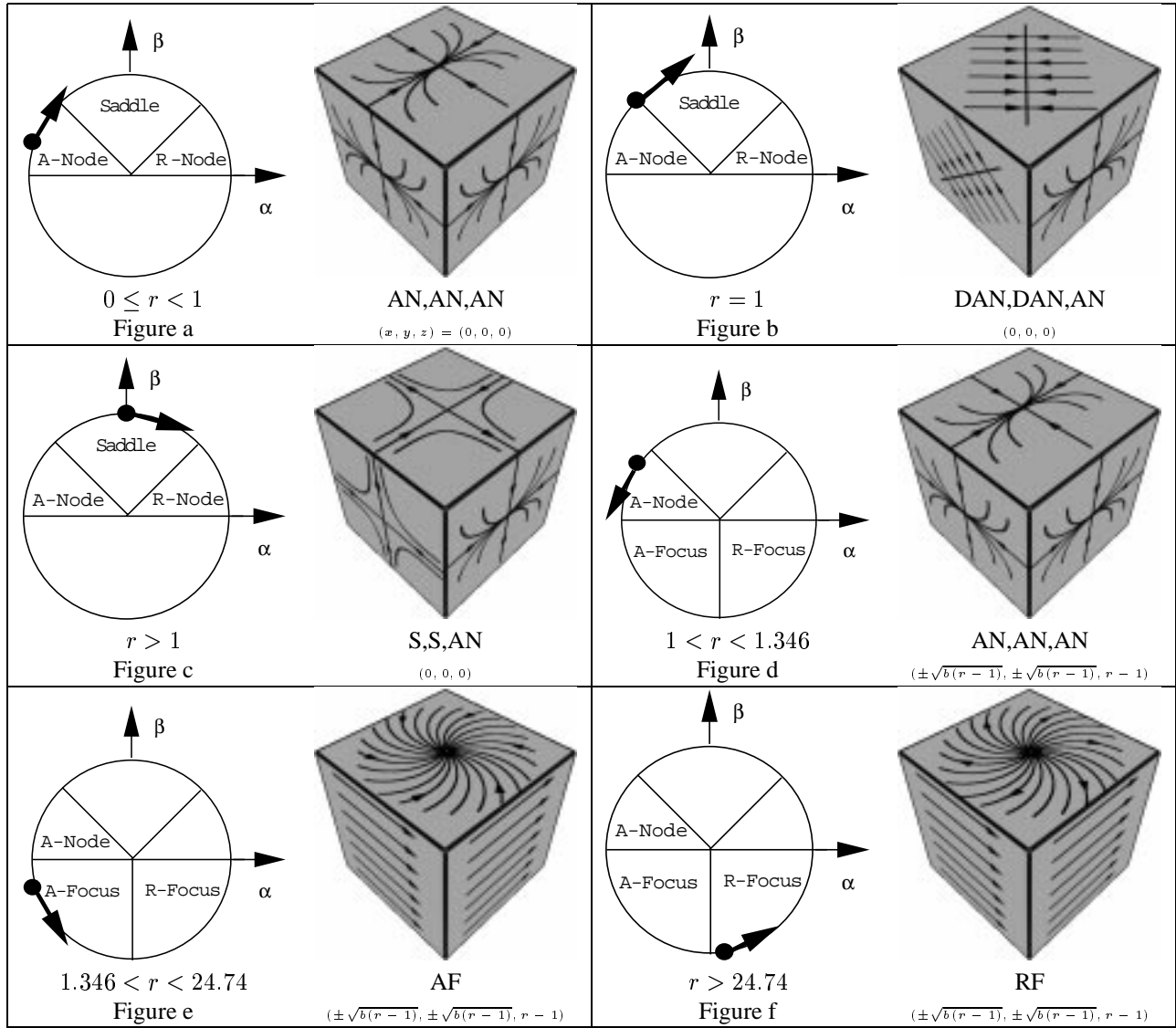
Figure 4: Lorenz Model for Fluid Convection depicted in α, β space. $\sigma = 10, b = 8/3$. AN:Attracting Node, DAN:Degenerate Attracting Node, S:Saddle, AF:Attracting Focus, RF:Repelling Focus